CrossMark

Detecting Lipids on Planetary Surfaces with Laser Desorption Ionization Mass Spectrometry

Nikita J. Boeren[1,2] , Salome Gruchola[1] , Coenraad P. de Koning[1] , Peter Keresztes Schmidt[1] , Kristina A. Kipfer[1] , Niels F. W. Ligterink[1] , Marek Tulej[1] , Peter Wurz[1,2] , and Andreas Riedo[1,2]
[1] Space Research and Planetary Sciences, Physics Institute, University of Bern, 3012 Bern, Switzerland; nikita.boeren@unibe.ch
[2] NCCR PlanetS, University of Bern, 3012 Bern, Switzerland

Abstract

In the search for extraterrestrial life, biosignatures (e.g., organic molecules) play an important role, of which lipids are one considerable class. If detected, these molecules can be strong indicators of the presence of life, past or present, as they are ubiquitous in life on Earth. However, their detection is challenging, depending on, e.g., instrument performance, as well as the selected site. In this contribution, we demonstrate that, using laser desorption ionization mass spectrometry, detection of lipids is feasible. Using our space prototype instrument designed and built in-house, six representative lipids were successfully detected: cholecalciferol, phylloquinone, menadione, 17α-ethynylestradiol, α-tocopherol, and retinol, both as pure substances and as mixtures additionally containing amino acids or polycyclic aromatic hydrocarbons. Observed limits of detection for lipids already meet the requirements stated in the Enceladus Orbilander mission concept. The current performance of our LDI-MS system allows for the simultaneous identification of lipids, amino acids, and polycyclic aromatic hydrocarbons, using a single instrument. We therefore believe that the LDI-MS system is a promising candidate for future space exploration missions devoted to life detection.

Unified Astronomy Thesaurus concepts: Mass spectrometry (2094); Time-of-flight mass spectrometry (2222); Astrobiology (74); Biosignatures (2018); Space vehicle instruments (1548)

1. Introduction

As long as humanity has existed, it has wondered about its origin and its place in the universe (Popa 2004; Lingam & Loeb 2021). The confirmed existence or absence of extinct or extant extraterrestrial life would have an unimaginable impact on our ideas concerning the origin of life on Earth. The search for life in our solar system and beyond is therefore the main driving force in the field of astrobiology.

Historically, the search for life outside Earth has been mainly focused on our neighboring planets, primarily Mars (Klein 1979; de Morais & Teles 2015; Vago et al. 2017; Carrier et al. 2020). In the 1970s, the measurements performed during the Viking missions marked the first true search for extraterrestrial life (Soffen 1976, 1977; Soffen & Snyder 1976; Biemann et al. 1977). The results of these measurements, as well as the many measurements that followed by, e.g., the ExoMars program, Curiosity rover, and Mars 2020 Perseverance rover, have resulted in our current view that life on Mars would be restricted to locations sufficiently below the surface, protected from the harsh radiation and ionization environment on the surface (Onstott et al. 2019). For this reason and due to findings of other past missions, the astrobiological focus has started to shift toward other targets in the solar system as well.

Particularly interesting astrobiological targets have recently been identified in the form of the icy moons of Jupiter and Saturn, in particular Europa and Enceladus, respectively (Lunine 2017). Several of the large space agencies (e.g., NASA, ESA, JAXA) have recently launched and/or are

planning missions to these icy moons with the aim of assessing habitability and searching for signatures indicative of the presence of extinct or extant life (European Space Agency 2005; Grasset et al. 2013; Voyage 2050 Senior Committee 2021; National Academies of Sciences, Engineering, and Medicine 2022).

The presence of liquid water oceans underneath the kilometers-thick outer ice shells of Europa and Enceladus, as discovered by the Galileo mission (Carr et al. 1998; Kivelson et al. 2000) and the Cassini Huygens mission (Porco et al. 2006; Waite et al. 2017), respectively, fueled the drive for further investigation with a dedicated focus on the search for extraterrestrial life (Lunine 2017). Several missions are currently being prepared to investigate Europa, including the JUICE/ESA (Grasset et al. 2013) and the Europa Clipper/NASA (Phillips & Pappalardo 2014; Pappalardo et al. 2021) missions. Missions to Enceladus have been proposed as well (Cable et al. 2021; MacKenzie et al. 2021), and recently NASA included the Enceladus Orbilander as a second-highest-priority flagship mission in their decadal strategy report (National Academies of Sciences, Engineering, and Medicine 2022).

These so-called ocean worlds are deemed targets of high potential for the detection of extraterrestrial life owing to the probable presence of all ingredients for life as we know it. Measurements of a plume of Enceladus have provided more insight into such ocean worlds (Waite et al. 2006). The plume mostly consists of water and also contains salts, silica nanoparticles, and organic compounds (Waite et al. 2009; Postberg et al. 2011, 2018; Hsu et al. 2015). These results show the probable presence of a saline ocean that is in direct contact with the core of Enceladus, as well as the presence of hydrothermal processes (Hsu et al. 2015; Sekine et al. 2015). These hydrothermal vents in the ocean bed could be an energy

source (Hand et al. 2007; Deamer & Damer 2017; Steel et al. 2017; Damer & Deamer 2020), while simultaneously being a source of metabolic compounds for any tentatively present chemotrophic organisms (Schulze-Makuch & Irwin 2002; Ray et al. 2021).

It has been suggested that biosignatures of such life-forms can be sprayed out through cracks in the ice layer and be deposited onto the ice shell by plumes (Bywaters et al. 2020; National Academies of Sciences, Engineering, and Medicine 2022). Detection of these biosignatures would then likely be possible through analysis of redeposited material on the icy surface. Performing the required in situ measurements of subsurface ice or directly from the plume poses many challenges, including small sample volumes, flight-capable instrumentation able to withstand the harsh radiation environments present at these objects, and the severely limited information available on potentially present compounds, consequently targeting unknown compounds and compositions that may be present.

In the search for evidence of "life as know it," several classes and compounds of organic molecules are of bio-relevant interest and are of interest as potential biosignatures for space exploration missions. Characterization of these organics would be beneficial in determining the extent of organic chemistry present and would provide detailed information about the possible presence of life and environment (habitability). A Decadal Strategy for Planetary Science and Astrobiology 2023–2032 summarizes recommendations for investigation of organic biomolecules, including amino acids, sugars, nucleobases, and lipids, in solar system planetary environments for several future space missions (National Academies of Sciences, Engineering, and Medicine 2022). The degree of molecular complexity, such as size, presence of heteroatoms (e.g., O, N, S), molecular geometry, and presence of functional groups, is of relevance in distinguishing abiotic from biotic signatures.

Lipids are quintessential for life as we know it and are involved in cell structure and function. Lipids, which cover an extremely large range of molecules, have several subclasses that are deemed highly predictive for the presence of life (Fahy et al. 2009, 2009; Georgiou & Deamer 2014), specifically lipids that are involved in membrane formation and/or cell structure (Georgiou & Deamer 2014; Deamer 2017; Cavalazzi & Westall 2019). Among the lipids of interest are, for example, fatty acids, sterols and hopanoids, prenols (or isoprenoids), and carotenoids (National Research Council 2002; Waldbauer et al. 2011; Sáenz et al. 2012; Nakatani et al. 2014; Belin et al. 2018; Cavalazzi & Westall 2019; Jordan et al. 2019; Shen et al. 2020). This makes lipids a highly interesting and broad class of organic biosignatures to study further for future space missions aiming to detect signs of life.

Prenol lipids, sometimes classified as isoprenoids, play an important role in oxidative stress (Cavalazzi & Westall 2019; Jordan et al. 2019). Sterol lipids, sometimes referred to as polyisoprenoids or triterpenoids, are complex lipids involved in cell membrane flexibility and many regulatory and signaling processes (Ourisson & Nakatani 1994; Poger & Mark 2013; Cavalazzi & Westall 2019). Both prenol and sterol lipids are isoprene-based lipids and share a common biosynthesis pathway (Fahy et al. 2005). Sterol lipids are notably uniquely biogenic owing to their complexity, which cannot be arranged by simple chemical and physical processes. Not surprisingly, both prenol and sterol lipids are mentioned in several mission proposals and (strategy) reports to be of interest for detection of signs of life (National Research Council 2002; Hays 2015; Hand et al. 2017; Neveu et al. 2018).

During space exploration missions, a mass spectrometric instrument is commonly included in the payload for the detection of organic biosignatures, mostly due to the versatility of detection, its flexibility, and its wide applicability to many different chemical species (Hoffman et al. 2010; Arevalo et al. 2020). In addition, quantification of compounds using mass spectrometry is possible and a high dynamic range can be covered, which allows for analysis of trace species. Laser desorption ionization mass spectrometry (LDI-MS) is a flexible and adaptable technique for biosignature detection. Several mass spectrometers with a laser-based sampling system have been developed for space applications, such as CORALS, CosmOrbitrap, and L2MS (Anderson et al. 2012; Getty et al. 2012; Briois et al. 2016; Arevalo et al. 2018; Selliez et al. 2020; Willhite et al. 2021). Two LDI-MS instruments, DraMS and MOMA, are planned to be on the payload of future space missions for the detection and characterization of organics. MOMA will be on board the Rosalind Franklin Rover (ExoMars) planning to go to Mars and to be the first LDI-MS applied in space (Goetz et al. 2016; Li et al. 2017). DraMS is scheduled to be part of the Dragonfly mission to Titan set to launch in 2027 (Grubisic et al. 2021). All the different LDI-MS instruments vary in many components, including used laser source (e.g., wavelength or two-step desorption and ionization) and mass analyzer (e.g., Orbitrap^{TM} or time of flight). LDI-MS is not limited to a selected group of compounds but is capable of analyzing various compound groups, without the need for chemical alterations, e.g., derivatization using wet chemistry. Other advantages are the potential for high sensitivity and high spatial resolution, while not requiring/depending on consumables, such as carrier gas and columns for gas chromatography–mass spectrometry (GC-MS) analysis (Ligterink et al. 2020b).

Recently, our group developed a space prototype laser desorption ionization mass spectrometric system for the detection of biomolecules, called the ORganics Information Gathering INstrument (ORIGIN; Ligterink et al. 2020a). Previous studies using ORIGIN focused on the analysis of amino acids and polycyclic aromatic hydrocarbons (PAHs; Ligterink et al. 2020a, 2022; Kipfer et al. 2022; Schwander et al. 2022). Unique and simple mass fragmentation patterns were observed for the amino acids, allowing for robust identification and quantification, while limited fragmentation for PAHs was observed and parent ions were identified. The detection limits for both amino acids and PAHs were in the femtomol mm^{-2} range (Ligterink et al. 2020a; Kipfer et al. 2022). The influence of the presence of salt was investigated as well, as the presence of salt at percent level is expected on ocean worlds, and biosignature detection by current instruments, such as pyrolysis-GC-MS, can be extremely challenging in the presence of salt (Benner et al. 2000; Navarro-González et al. 2006; Montgomery et al. 2019). ORIGIN was shown to be unaffected by matrix composition changes through salts and/or surface minerals (Ligterink et al. 2020a). In addition, identification of amino acids in complex natural samples was investigated using a correlation network analysis method to separate amino acid signatures from soil signatures (Schwander et al. 2022). The versatile capabilities of ORIGIN with respect to implementing the technique on a Venus Life Finder mission
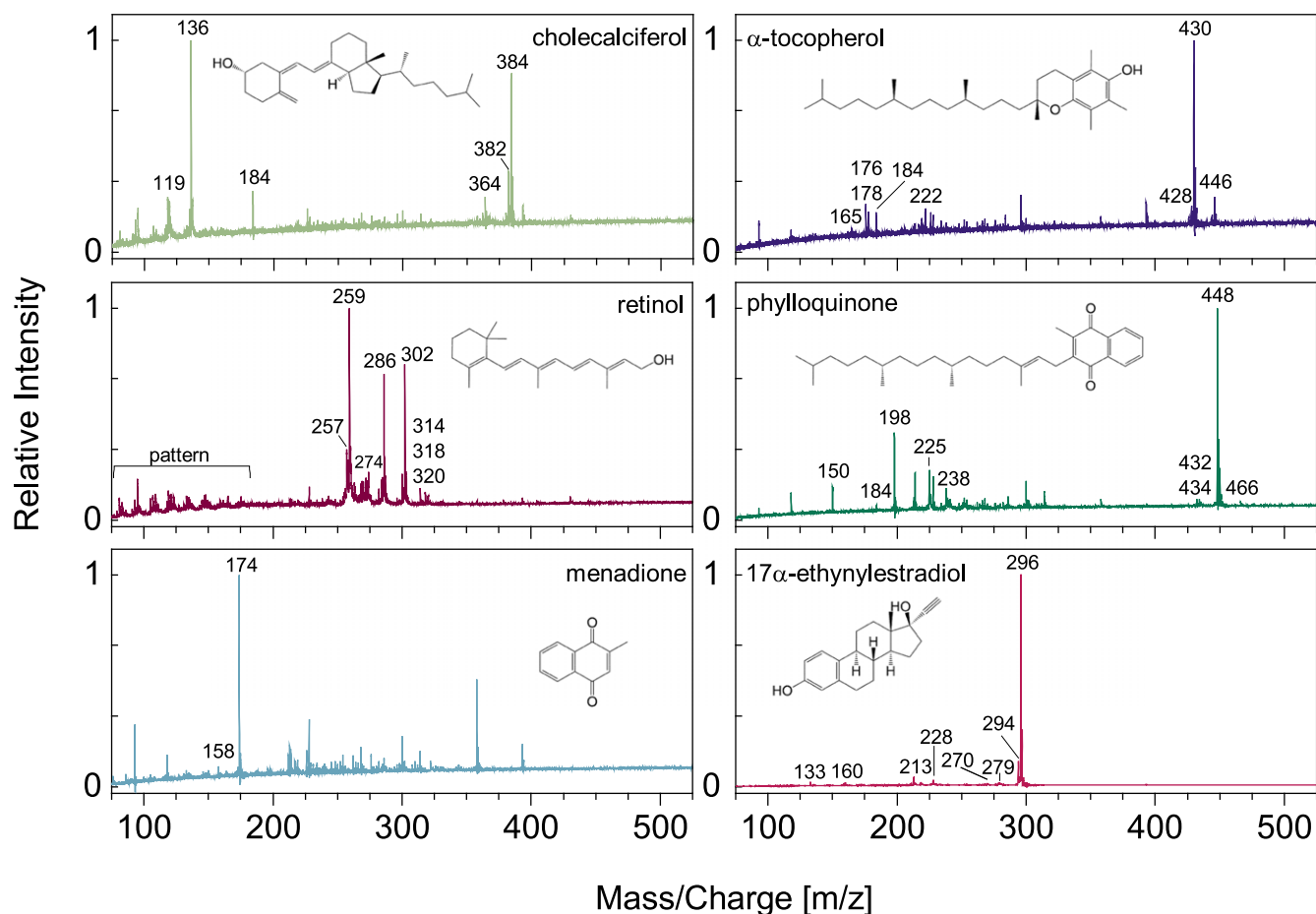
Figure 1. Mass spectra of cholecalciferol, α-tocopherol, retinol, phylloquinone, menadione, and 17α-ethynylestradiol standards. Identified lipid and fragment peaks are annotated with their mass-to-charge ratio [m/z] expressed as integers, and molecular structures of each lipid are given in the corresponding mass spectrum.

and other future mission opportunities have been discussed as well (Ligterink et al. 2022).

This study was conducted to test the detection capabilities of ORIGIN toward lipids, specifically prenol and sterol lipids, for in situ measurements on planetary surfaces or fly-by plume probing. The results presented are discussed in the context of future space exploration missions searching for signs of (extinct or extant) life on ocean worlds.

2. Material and Methods

2.1. Sample Material

In this study, the lipid standards cholecalciferol (384.64 g mol^{-1}), phylloquinone (450.70 g mol^{-1}), menadione (172.18 g mol^{-1}), 17α-ethynylestradiol (296.40 g mol^{-1}), α-tocopherol (430.71 g mol^{-1}), and retinol (286.45 g mol^{-1}) were investigated (see Figure 1 for molecular structures). The standards were all purchased at Sigma-Aldrich (purity ⩾95%). While several of the selected lipids are not directly involved in biological processes, they are very suitable as analogous material for proof-of-concept measurements, and with the advantage of being readily available.

2.2. Sample Preparation

All tools used for sample preparation were flame sterilized before usage. High-purity Eppendorf tubes and pipetting tips

(both Biopur® grade) were used for stock solution preparation to avoid sample contamination.

First, the lipid standards were dissolved in isopropanol (LC-MS grade, Merck kGaA) at a concentration of 400 μM as standard stock solutions. Samples were prepared by dilution of the stock solutions to the desired concentration with a final total solvent ratio of 1:1 isopropanol:water (milliQ water, 18.2 MΩ·cm). An isopropanol:water (1:1) solution subjected to all sample preparation and dilution steps, but lacking any analyte, served as blank.

Three sample mixture solutions were prepared by mixing stock solutions in the Eppendorf tubes and subsequently diluting to the appropriate concentration for measurement. The first mixture contained cholecalciferol, phylloquinone, menadione, 17α-ethynylestradiol, α-tocopherol, and retinol and was prepared with a concentration of 50 μM of each lipid in isopropanol. The second mixture contained both amino acids (investigated recently; see Ligterink et al. 2020a) and lipids. Amino acid stock solutions of 400 μM in water were prepared for two amino acids, namely, histidine and methionine (Sigma-Aldrich, ⩾99.5%, both). A mixture containing these two amino acids and four lipids (cholecalciferol, phylloquinone, 17α-ethynylestradiol, α-tocopherol) was prepared with a final concentration of 50 μM for each compound using a 1:1 isopropanol:water mixture as solvent. The third mixture consisted of two PAHs (investigated recently; see Kipfer et al. 2022), namely, coronene and perylene, and four lipids

(cholecalciferol, phylloquinone, 17α-ethynylestradiol, α-tocopherol) in isopropanol:heptane (1:1) at a final concentration of 25 μM for the PAHs and 50 μM for the lipids. Note that amino acids and PAHs could not be prepared in one sample mixture, due to insolubility of PAHs with any amount of water.

Platinum-coated silicon wafers (Pt wafers) were used as sample substrate, which were fixed onto a stainless steel holder with carbon tape for vacuum application. 1 μL of a prepared sample solution was drop-cast on the surface, and the sample was left to evaporate the solvent. After about 30 minutes, the sample residue on the holder was placed in the vacuum chamber of ORIGIN for measurement. All sample preparation steps, including evaporation of solvent from the sample holder, were performed in a laminar flow bench (ISO5) to minimize contamination.

Concentration scans for three lipids, phylloquinone, 17α-ethynylestradiol, and α-tocopherol, were measured on a stainless steel sample holder instead of using the Pt wafers. A stainless steel disk with 0.2 mm deep cavities of 3 mm in diameter was used as sample holder substrate. In comparison to the Pt sample substrates, the cavities allowed for accurate average surface concentration calculations (see also Ligterink et al. 2020a). Sample preparation was performed as described previously, only the sample solutions were drop-cast into the cavities.

2.3. ORIGIN Instrumental Setup

ORIGIN is a laser desorption ionization mass spectrometer (Ligterink et al. 2020a). The instrument consists of a miniature reflectron-type time-of-flight (R-TOF) mass analyzer that separates cations based on their flight time, which relates to their mass-to-charge ratio (m/z).

Sample desorption and ionization is performed by a Q-switched Nd:YAG laser system (Quantel Brio) with a pulse width of about 3 ns, laser wavelength of 266 nm, and laser pulse repetition rate of 20 Hz. The focused pulsed laser beam is guided through a vacuum entrance window toward the sample surface while passing through the R-TOF along the central axis.

The sample holder is placed on an X, Y, Z translational stage (Agilis, Newport) inside the vacuum chamber below the miniature R-TOF. A multichannel plate detector system (MCP) produces an analog signal in response to incoming ions, which is digitalized by a high-speed analog-to-digital converter card (U1084A, Agilent) with a selected sampling rate of 2 GS s^{-1}, yielding time-of-flight spectra with a length of 20 μs. A more detailed description of the instrument setup can be found in Ligterink et al. (2020a).

2.4. Measurement Procedure

Prior to placing the sample holder into the vacuum chamber, the chamber was vented with high-purity nitrogen (Alphagaz 2, Carbagas). The sample holder was placed on the stage, below the R-TOF instrument, and the chamber was evacuated to a pressure below 10^{-7} mbar within several hours. A standard measurement procedure was used for all measurements. Measurements were performed with a laser pulse energy of $\sim$3 μJ on the surface, unless specified differently. This pulse energy was selected to allow for direct comparison with previous measurements of different compounds and to also assess the applicability of the measurement protocol

(Ligterink et al. 2020a; Kipfer et al. 2022). A scan of laser power was performed for the cholecalciferol sample to evaluate the suitability of the laser pulse energy (see Appendix A). The MCP detector was operated at 2250 V.

To account for inhomogeneity in residue deposition during evaporation of the solvent and to facilitate statistical calculations, a single measurement run comprised sampling of 40 positions on the sample, spaced linearly with a distance of about 50 μm. At each position, 100 laser shots were applied, resulting in a total of 4000 TOF spectra for each measurement. This set of spectra enables a reliable and more accurate analysis compared to single-shot spectrum analysis. A single measurement covering 4000 spectra took approximately 7 minutes and covered a mass range up to around m/z 700.

2.5. Data Analysis

Data analysis was performed using an in-house-developed Matlab software suite (Meyer et al. 2017). For each measurement position, every spectrum with a signal-to-noise ratio (S/N) $\geqslant$ 6 of the 4000 spectra was co-added to a single TOF spectrum to yield a single time spectrum. Conversion from time spectrum to mass spectrum was subsequently performed through calibration using peaks with a known mass spread over the spectrum, e.g., ^{23}Na^{+} at m/z 23 on the low-mass side. Thereafter, Simpson integration was performed for each peak using automatic integration window selection and background correction (Meyer et al. 2017).

Additional peak characteristics, such as the S/N of peaks and mass resolution [$m/\Delta m$], were calculated for each peak. Blank measurements were used to identify peaks contributed by contaminants from the sample preparation or sample holder material, to omit them from further analysis.

Limits of detection (LODs) were determined for three lipids, 17α-ethynylestradiol, phylloquinone, and α-tocopherol, based on the measured concentration scans. By extrapolation of the regression line to the signal ($y = a + bx$) down to the 3σ noise level, the LOD value was calculated using

$$\text{LOD}_{3\sigma} = \frac{\frac{1}{n}\sum_{j=1}^{n}\left(3\bullet\sqrt{\frac{1}{N-1}\sum_{i=1}^{N}|A_i - \mu|^2}\right)_j - a}{b}, \quad (1)$$

where n denotes the number of spectra, N the number of data points in a spectrum, A_i the intensity of species i [a.u.], μ mean of the noise, and a the intercept and b the slope of the linear regression line.

3. Results

3.1. Peak Identification of Lipid Standards

Figure 1 depicts mass spectra recorded from the six lipid standards of cholecalciferol, α-tocopherol, retinol, phylloquinone, menadione, and 17α-ethynylestradiol. Multiple mass peaks are identified for each lipid associated with the parent ion and fragment ions of the lipid. In Appendix A, a mass spectrum of a blank measurement (Figure 6) is shown, which was used to facilitate background identification. Figure 1 shows that each molecule has its own identifiable mass spectrometric pattern, with the parent mass and a few fragment peaks. For the lipids cholecalciferol, a-tocopherol, retinol, and 17α-ethynylestradiol, the parent ion could be observed, namely, at m/z 384, 430, 286, and 296, respectively. For phylloquinone, m/z 448 was
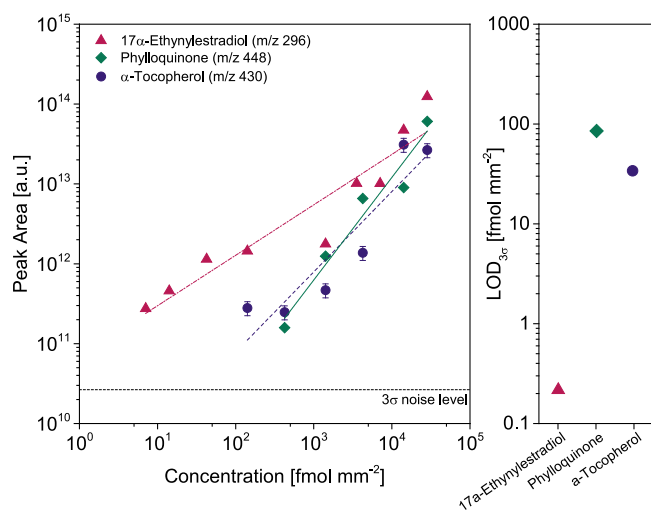
Figure 2. Left: concentration scans of 17α-ethynylestradiol, phylloquinone, and α-tocopherol with observed peak area to surface area concentration [fmol mm^{-2}]. The linear regression line ($y = a + bx$, where $y = \log$(Peak Area) and $x = \log$(Concentration)) for each lipid is also shown. Right: theoretical LODs for each investigated lipid given in fmol mm^{-2}. The LOD value is obtained by extrapolating linear regression lines down to the 3σ noise level.

the main peak observed, corresponding to $[\mathrm{M}-2]^+$, whereas for menadione m/z 174 was the main peak observed, corresponding to $[\mathrm{M}+2]^+$. A parent ion peak was observed for both phylloquinone and menadione with very low signal intensity. Fragment ions can be observed at various degrees for the different molecules.

3.2. Quantification and Limit of Detection

To assess the detection and quantification capabilities of ORIGIN, concentration scans of three different lipids were measured. To allow for a more accurate determination of the average surface concentration of the sample, these measurements were performed on a stainless steel sample holder with premade cavities instead of the Pt wafers used in the previous measurements. The cavities in the steel disk allowed for more consistency between different measurements and facilitated accurate sample surface area determination.

Sample solutions of different concentrations of 17α-ethynylestradiol, phylloquinone, and α-tocopherol were drop-cast to yield a range of surface concentrations between 7 fmol mm^{-2} and 28 pmol mm^{-2}. The left panel of Figure 2 shows resulting peak areas of a single peak for each lipid at the different surface concentrations. The selected mass peaks were m/z 296, m/z 448, and m/z 430 for 17α-ethynylestradiol, phylloquinone, and α-tocopherol, respectively. The selected mass peaks represent the most prominent peak observed in the mass spectrum for each of the lipids to facilitate low-concentration measurements.

$\mathrm{LOD}_{3\sigma}$ was derived by extrapolating a linear regression through the measured points down to the 3σ noise level. In the right panel of Figure 2, the $\mathrm{LOD}_{3\sigma}$ of the three different lipids is shown. An $\mathrm{LOD}_{3\sigma}$ of 0.2 fmol mm^{-2} for 17α-ethynylestradiol was observed, 85 fmol mm^{-2} for phylloquinone, and 34 fmol mm^{-2} for α-tocopherol. Note that the stated value for $\mathrm{LOD}_{3\sigma}$ assumes no isobaric interference of any kind at the selected mass peak.

## 3.3. Effect on Sample Surface Substrate and Lipid Detection

Generally, the Pt-coated substrate was used as sample substrate for laser desorption and ionization of the analytes. Only the concentration scans were measured on stainless steel to allow for more accurate average surface concentration calculations due to the presence of cavities. A comparison between the different substrates can be made to investigate influence of the substrate and to assess the robustness of the method. Figure 3 shows mass spectra of four different lipids measured on both Pt-coated and stainless steel substrates, and mass spectra of blank measurements are given in Appendix A (Figures 6 and 7).

A high similarity between the mass spectra of the lipids is observed for the different substrates. Parent ion peaks were observed for all four lipids on both substrates, and the fragment peaks appear at the same m/z values. Despite the resemblance of the mass spectra from two substrates, interesting differences are observed between the Pt-coated and stainless steel surfaces. A difference in peak ratio is seen, which is most apparent for phylloquinone. For phylloquinone, higher fragmentation is observed on the steel substrate in the lower-mass region (e.g., m/z 198), as well as an increase of ratio of the molecular ion peak (m/z 450) compared to the $[\mathrm{M}-2]^+$ peak at m/z 448 (see Figure 11 in Appendix A for a zoom-in of the spectrum). Another apparent dissimilarity is the difference in adduct formation $[\mathrm{M}+16]^+$ of α-tocopherol. This is most likely due to oxidation and was increased in measurements on the platinum surface of α-tocopherol. This adduct formation was also observed for phylloquinone, but no apparent difference between the substrates was observed. For both sterol lipids, 17α-ethynylstradiol and cholecalciferol, no $[\mathrm{M}+16]^+$ peak was observed.

3.4. Mixture Measurements

Three different mixtures containing lipids, amino acids, and/or PAHs were measured to investigate whether the presence of different classes of biosignatures can be detected and identified simultaneously. These mass spectra are shown in Figure 4, with symbols denoting peaks attributed to a specific molecule based on mass spectra obtained for pure compounds. All compounds, except menadione (lipid) and methionine (AA), could be identified in the mixtures. Menadione and methionine showed low signal intensity in previous measurements on single compounds; thus, their signal is probably too low to rise above the background. Several peaks (e.g., m/z 93) could not be attributed to any of the investigated compounds and are therefore assumed to be due to either contamination or fragment recombination.

A difference in signal intensity is observed between the different compounds, as is expected from the measurements of the pure compounds. In particular, PAHs (m/z 300 and m/z 252) are very prominent in the spectrum, as well as phylloquinone (m/z 198), histidine (m/z 156), and 17α-ethynylestradiol (m/z 296). These compounds have in common that they are aromatic-ring-based structures and thus show in general high UV absorption. However, not only can UV absorption have an effect on the signal intensity, but other effects may exist as well, such as first-order ionization efficiency and surface effects like absorbance (and perhaps also shielding) of the substrate, including heating of the surface.
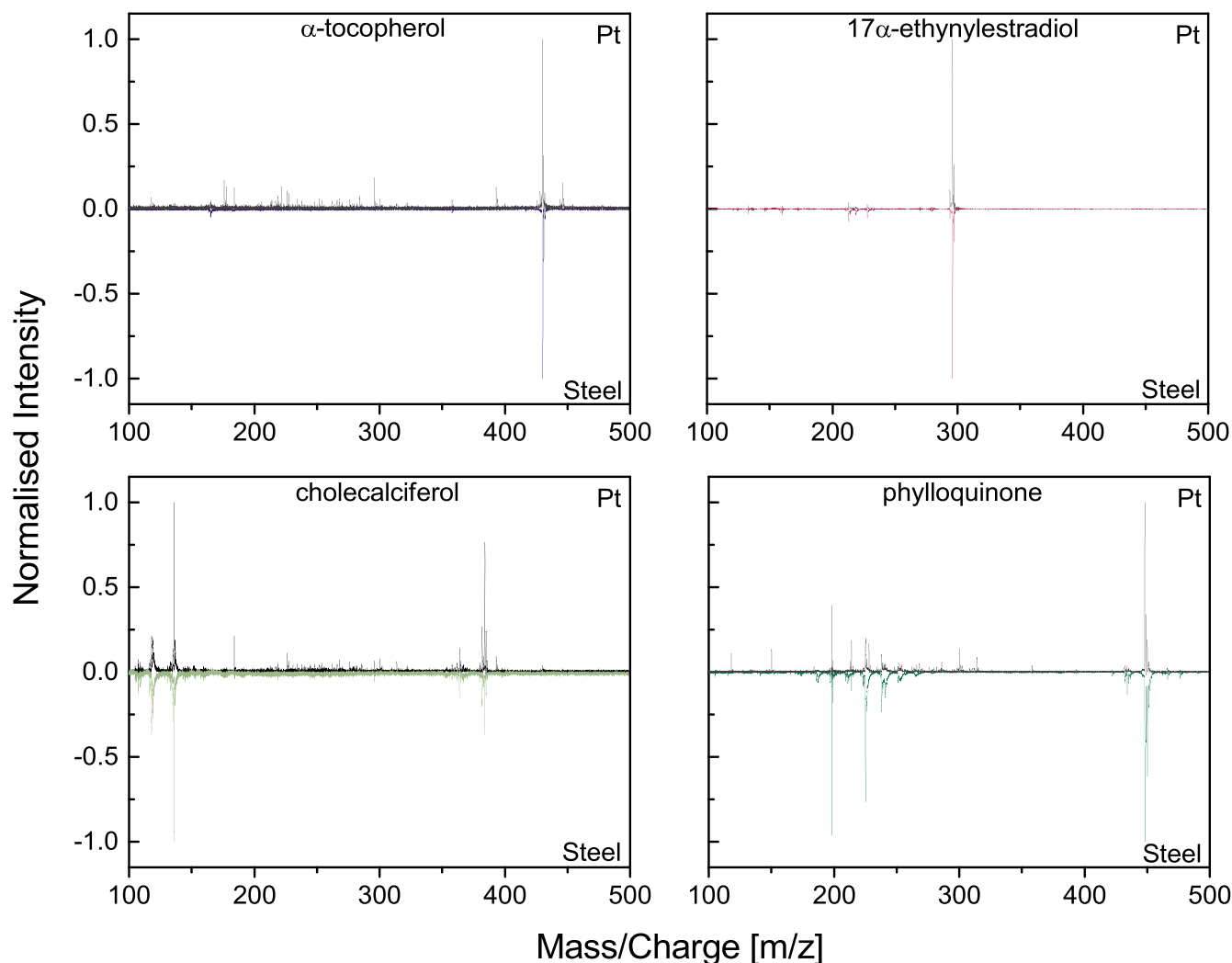
Figure 3. Comparison of mass spectra for a platinum-coated and a stainless steel sample substrate for α-tocopherol, 17α-ethynylestradiol, cholecalciferol, and phylloquinone. All measurements were performed with a 3 μJ laser pulse energy.

Overlapping masses between lipids, amino acids, and PAHs are inevitable, but this has been shown not to be a problem in this study. Peaks were well separated, and no isobaric interference was observed. For example, peaks from 17α-ethynylestradiol at m/z 296 and coronene at m/z 300 were well separated from each other. In these higher mass ranges, a mass resolution [$m/\Delta m$] around 1100 was achieved.

4. Discussion

Measurement capabilities of ORIGIN of prenol and sterol lipids have been demonstrated in this study. Measurements of different mixtures indicate that a broad range of complex molecules, namely, lipids, amino acids, and PAHs, can be detected and identified simultaneously with the ORIGIN setup using a single instrument setup and measurement procedure. Parent ions could be identified for all lipids (also considering [M+2H]$^+$ and [M−2H]$^+$ peaks), and fragment ions were observed for each lipid as well, creating a mass spectrometric pattern that can be used for their identification in complex mixtures. Some typical detected fragments for the lipids are in agreement with mass spectra stored in the NIST Mass Spectral Library, like m/z 198 for phylloquinone and the pattern for retinol in the lower mass range (National Institute of Standards and Technology 2021a, 2021b). Even though this carbon-chain pattern is not specific for retinol only, in this study retinol has the most distinguishable pattern. The peak at m/z 198 for phylloquinone is thought to be a fragment of breaking/cleaving off the long aliphatic carbon chain at the location of the double bond (see Appendix B for proposed fragmentation site).

Mass peaks with a difference of 2 Da compared to the nominal parent ion mass were observed for all lipids. Most lipids showed only a low-intensity peak at [M−2H]$^+$, with two exceptions. For phylloquinone [M−2H]$^+$ was the main contributing peak, while for menadione [M+2H]$^+$ was mainly observed. The difference in observed ion mass is attributed to addition or abstraction reactions during laser desorption. In our study, this might be enhanced by the use of a platinum surface as sample holder introducing catalytic reactions in the desorbed plume of material.

Adduct formation of [M+16]$^+$ was observed for several lipids as well, i.e., phylloquinone, α-tocopherol, and retinol, which is most likely due to oxidation of the lipid. In our previous studies on amino acids and PAHs, oxidation adducts were not observed (Ligterink et al. 2020a; Kipfer et al. 2022). Mass spectra of amino acids showed mostly loss of the acid group, while PAHs were very stable, with limited fragmentation and various extents of cluster formation (Kipfer et al. 2022).
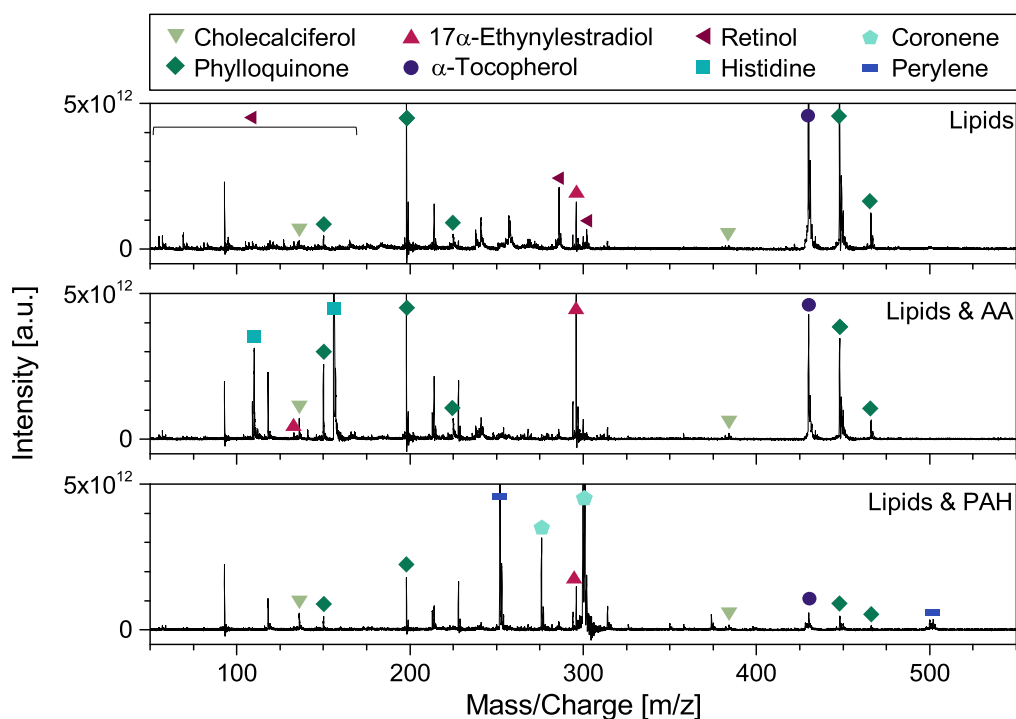
Figure 4. Mass spectra of three different mixtures, namely, six lipids (top), four lipids and two amino acids (middle), and four lipids and two PAHs (bottom). Intensity was cut off at 5×10^{12} to also show lower-intensity peaks, and peaks corresponding to the different compounds are annotated by symbols.

While fragmentation was also observed for the lipids in this study, the observation of their parent ions indicates more stability during laser desorption and ionization compared to amino acids.

In all mass spectra, contamination of the sample holder substrate is seen in the form of numerous low-intensity peaks present at many m/z values, especially in the mass range below m/z 100 and between m/z 200 and 300. These background peaks were suppressed in the presence of sample material, especially if the compound was well desorbed and ionized, e.g., in the mass spectrum of 17α-ethynylestradiol. Moreover, some observed contaminant peaks were higher in blank measurements compared to when an analyte was present. This could be due to the thin sample film shielding the substrate surface from the incoming laser pulses, thereby preventing contaminant compounds from being desorbed. While in this study the background due to contamination did not influence identification, contaminations need to be reduced to minimize potential isobaric interferences, thus improving the LOD, especially when considering complex natural samples.

Two different sample surface substrates, Pt-coated silicon wafers and stainless steel, were used in this study. The stainless steel substrate was used for concentration scans because it allowed for a more accurate determination of the average surface concentration of the samples owing to the presence of milled cavities. However, the use of this steel substrate comes with several disadvantages. First, the manufacturing process involves lubricants, leading potentially to isobaric interferences with some analyte peaks. The removal of these lubricants to the required level (i.e., no observed signal) has proven to be extremely challenging, indicating that the lubricants are introduced deeply into the substrate material. Second, the manufacturing process (milling, grinding, cutting) creates a coarse surface with deep grooves and ridges, in which sample

buildup and/or carryover can happen. Clearly, there is an incentive to use substrates with a flat surface that can also be more rigorously cleaned (e.g., with strong acids) than stainless steel if needed, such as the Pt-coated substrates used in this study.

A comparison between the two different sample surface substrates, Pt-coated and stainless steel, was made (see Figure 3) to investigate the effect of the surface on the analysis. Desorption and ionization of the same lipids on different sample substrates resulted in very similar mass spectra. Obtaining consistent results while changing such a considerable component of the analysis method indicates robustness of the overall analysis method. Nevertheless, some minor differences between the mass spectra on different substrates were observed in terms of peak ratios (fragmentation patterns) and adduct formation by oxidation. These differences between the substrates could result from many factors, including differences in heating of the surface, wavelength absorption, and/or chemical properties of the surface. More thorough investigation into the contribution of the substrate surface is necessary to evaluate the influence of the laser desorption and ionization, but that was out of scope for this study.

The concentration scans exemplify the high dynamic range of ORIGIN, with a covered range of concentrations spanning over four orders of magnitude. All measurements were obtained with an identical measurement protocol and instrument settings. The current results indicate that quantitative information can be derived with order-of-magnitude accuracy from such calibration lines. The linear correlation observed for higher concentrations has a slight bend for lower concentrations, as seen in Figure 2, specifically for α-tocopherol. In general, laser desorption is not a quantitative process, but through the applied measurement protocol based on a statistical

approach (up to 4000 spectra are recorded per sample), quantitative information at the order of magnitude can be derived through calibration.

Theoretical LODs were calculated to be 0.2 fmol mm^{-2} for 17α-ethynylestradiol, 85 fmol mm^{-2} for phylloquinone, and 34 fmol mm^{-2} for α-tocopherol. The difference in LOD values between the different lipids is expected as is normally the case for different molecules. This was also observed in previous studies (Ligterink et al. 2020a), and scaling coefficients could be used for quantification between different compounds. An LOD below 100 fmol mm^{-2} was observed for all three lipids, corresponding to roughly an LOD below $\sim 7 \times 10^{-13}$ mol μL^{-1}. This LOD meets the requirements stated in the Enceladus Orbilander mission concept (1×10^{-12} mol μL^{-1}), which are based on concentrations realistically expected to be present on Enceladus should life be present. The sensitivity of ORIGIN can be further increased by optimizing the system, such as increasing the gain of the multichannel plate detector. An increase of 50 V of the MCP detector voltage leads roughly to a twofold signal amplification, which will aid low-concentration measurements even further (Riedo et al. 2017). In addition, the sample volume to surface area can be adapted to facilitate a concentration step and allow for more flexibility, since only one microliter of sample is drop-cast on to the sample substrate.

Lipids are important organic biosignatures to target for future space exploration missions searching for signs of (extinct or extant) life on ocean worlds. Various, mission-specific requirements are set for applicable in situ instrumentation, for example, a certain mass range ($\geqslant$500 Da) and LOD (compound group specific; MacKenzie et al. 2020). A mass range up to $m/z \sim 700$ is covered with current measurement procedures using the ORIGIN prototype instrument, and LOD requirements with respect to lipids are also met regarding the Enceladus Orbilander mission. Identification of prenol and sterol lipids was possible without the need for chemical alterations and/or liquid extraction. However, implementation of a general lipid extraction method for solids on future missions, such as ExCALiBR, would be beneficial (Wilhelm et al. 2020). This method would concentrate the lipid analyte further and, as a result, would increase the detection sensitivity of ORIGIN.

5. Conclusion and Outlook

This study demonstrates the measurement capabilities of ORIGIN for the detection of prenol and sterol lipids. Mass spectrometric patterns can be used for identification purposes, while quantitative information can be derived as well. A broad dynamic range over four orders of magnitude can be covered, and LODs were in the fmol mm^{-2} range.

Several classes of compounds relevant to biosignatures detection were measured using a single measurement procedure and instrument setup. ORIGIN is capable of measuring amino acids, PAHs, and lipids simultaneously. This shows the applicability of ORIGIN in upcoming missions for the detection of life, specifically for a mission to ocean worlds such as Enceladus or Europa.

As a first step, a specific, yet representative, subset of lipids was measured for this study, while lipids encompass a very broad range of biomolecules. Future studies will focus on other classes of lipids and other biosignatures as well. More investigation into the influence of the sample holder substrate with respect to the laser desorption and ionization is necessary as well, while it is thought that heating of the surface is playing a significant role as well in the desorption and fragmentation process.

Appendix A
Mass Spectra

Mass spectra that were not included in the main text are collected in this appendix. In Figure 5, a laser power scan measurement is shown of cholecalciferol. Spectra were collected at four different laser powers, as indicated in the figure. Figure 6 depicts a mass spectrum of a blank measurement on a platinum-coated silicon wafer, while Figure 7 depicts a mass spectrum of a blank on the stainless steel sample holder. Figures 8–11 show zoom-ins of Figure 3 focused on the molecular ion peak with adducts. These figures show a comparison between the Pt wafers and stainless steel substrate for four different lipids.
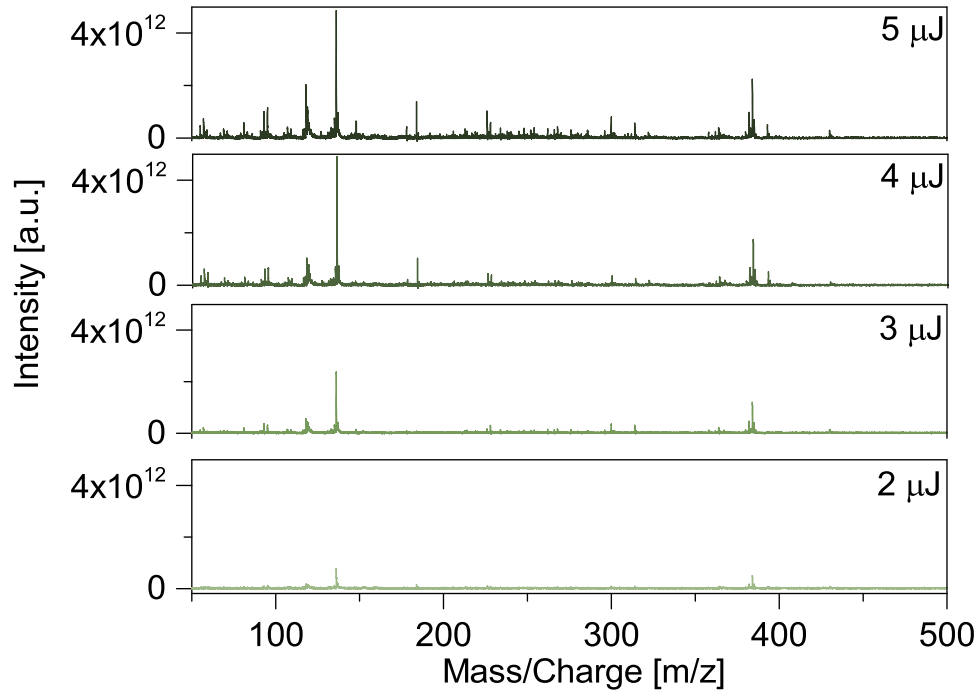

Figure 5. Scan of laser power for cholecalciferol (concentration 200 μM, on platinum-coated substrate) with applied laser pulse energies of 2, 3, 4, 5 μJ. Signal intensity is very low at low laser power, while high power introduces a lot of background peaks. Pulse energy of 3 μJ was selected for the other measurements to allow for direct comparison with previous measurements of different compounds and to also assess the applicability of the measurement protocol, while also being the trade-off between signal intensity and background noise.
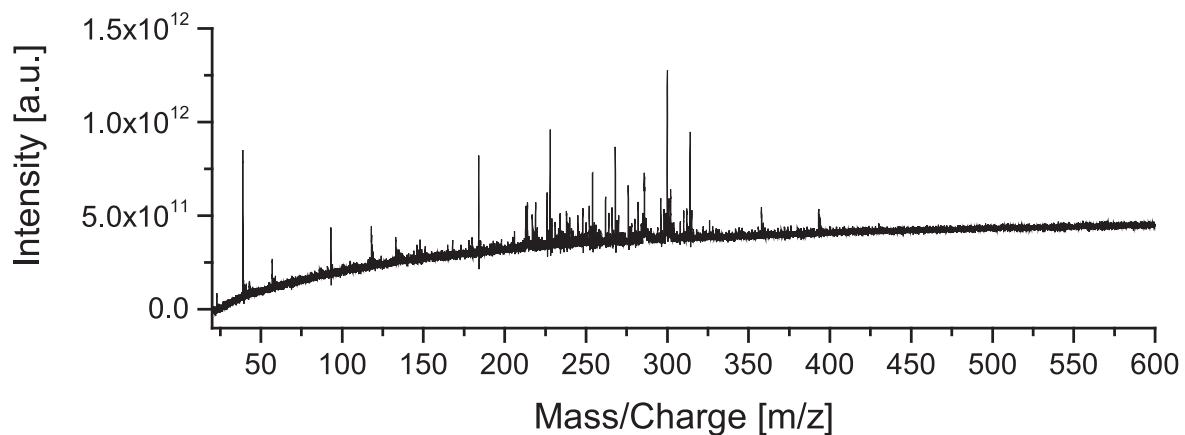

Figure 6. Mass spectrum of a blank measurement on the platinum-coated silicon substrate. A pulse energy of 3 μJ was applied.
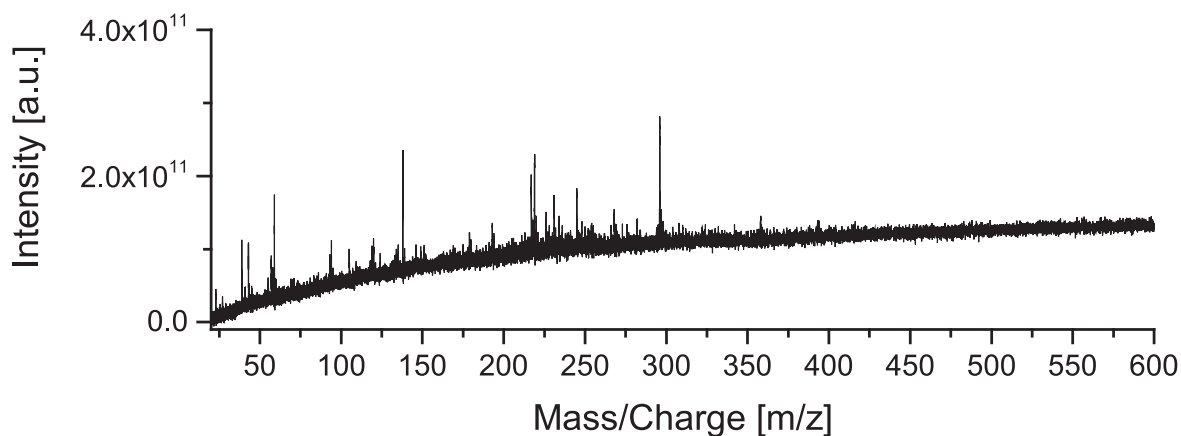
Figure 7. Mass spectrum of a blank measurement on the stainless steel sample substrate. A pulse energy of 3 μJ was applied.
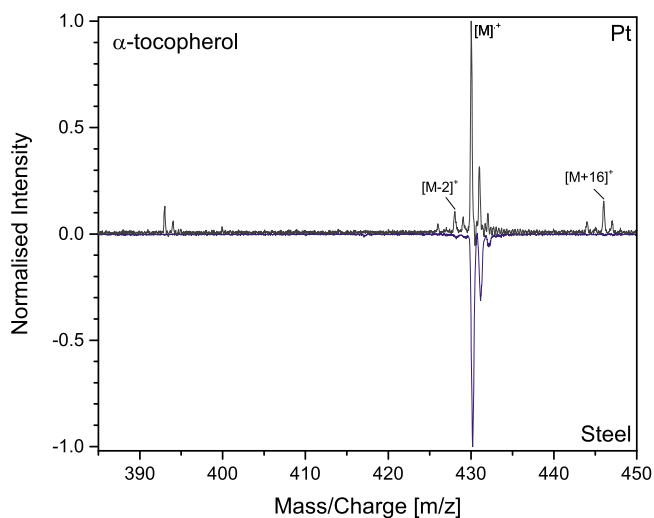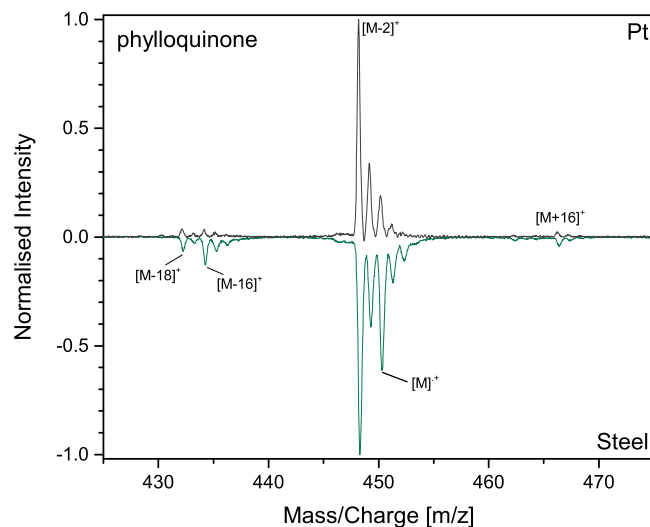

Figure 8. Zoom-in of the mass spectrum of α-tocopherol shown in Figure 3 of the comparison between a platinum-coated (pointing upward) and a stainless steel (pointing downward) sample substrate. Measurements were performed with a 3 μJ laser pulse energy.
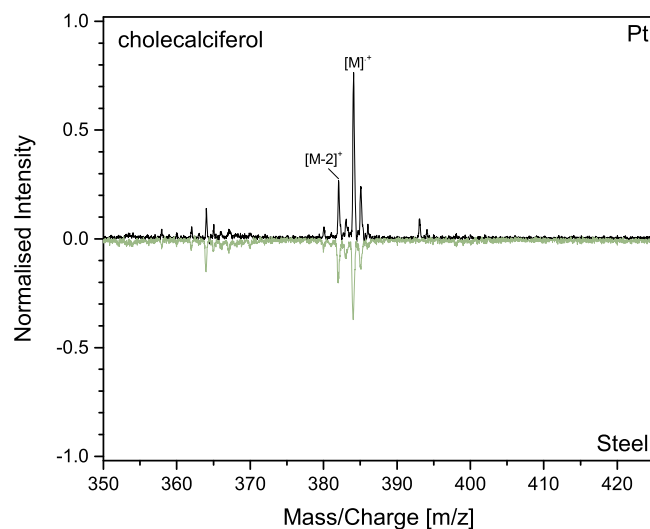
Figure 10. Zoom-in of the mass spectrum of cholecalciferol shown in Figure 3 of the comparison between a platinum-coated (pointing upward) and a stainless steel (pointing downward) sample substrate. Measurements were performed with a 3 μJ laser pulse energy.
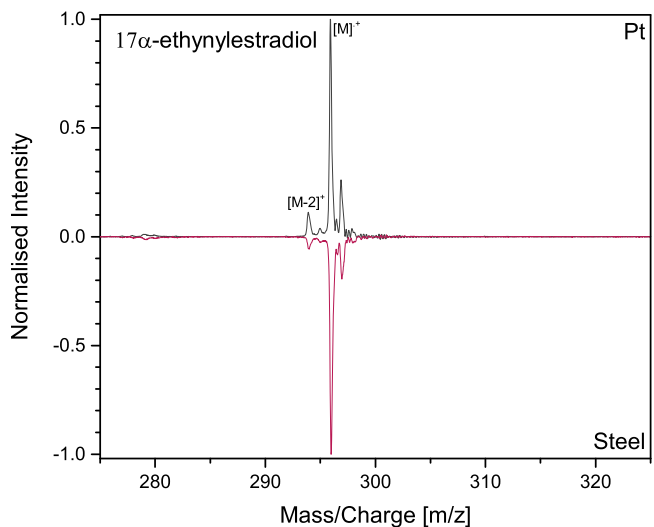

Figure 9. Zoom-in of the mass spectrum of 17α-ethynylestradiol shown in Figure 3 of the comparison between a platinum-coated (pointing upward) and a stainless steel (pointing downward) sample substrate. Measurements were performed with a 3 μJ laser pulse energy.

Figure 11. Zoom-in of the mass spectrum of phylloquinone shown in Figure 3 of the comparison between a platinum-coated (pointing upward) and a stainless steel (pointing downward) sample substrate. Measurements were performed with a 3 μJ laser pulse energy.

Appendix B
Fragmentation

In this appendix, suggested fragmentation sites for phylloquinone are given. Figure 12 indicates two fragmentation sites that could result in the peaks observed at m/z 198 and m/z 225 in Figure 1.
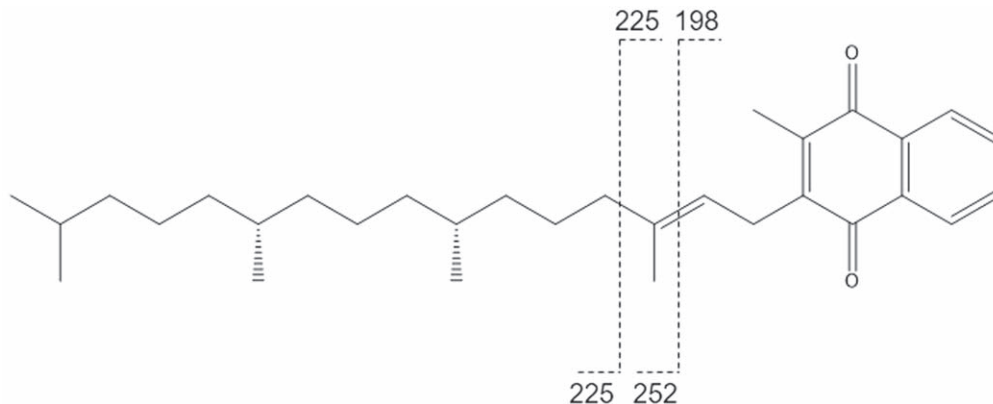
Figure 12. Chemical structure of phylloquinone with two proposed fragmentation sites indicated by the dashed lines. Numbers indicate the fragment size in Dalton (expressed as integers), with top numbers corresponding to the right side of the molecule and bottom numbers to the left side.

ORCID iDs

Nikita J. Boeren ⓘ https://orcid.org/0000-0001-6162-6953
Salome Gruchola ⓘ https://orcid.org/0000-0002-9757-1402
Coenraad P. de Koning ⓘ https://orcid.org/0000-0002-2540-7689
Peter Keresztes Schmidt ⓘ https://orcid.org/0000-0002-4519-8861
Kristina A. Kipfer ⓘ https://orcid.org/0000-0002-6544-9824
Niels F. W. Ligterink ⓘ https://orcid.org/0000-0002-8385-9149
Marek Tulej ⓘ https://orcid.org/0000-0001-9823-6510
Peter Wurz ⓘ https://orcid.org/0000-0002-2603-1169
Andreas Riedo ⓘ https://orcid.org/0000-0001-9007-5791

References

Anderson, F. S., Mahoney, J., Waite, H., et al. 2012, in 2012 IEEE Aerospace Conf. (Piscataway, NJ: IEEE), 1
Arevalo, R., Jr., Ni, Z., & Danell, R. M. 2020, JMSp, 55, e4454
Arevalo, R., Jr., Selliez, L., Briois, C., et al. 2018, RCMS, 32, 1875
Belin, B. J., Busset, N., Giraud, E., et al. 2018, Nat. Rev. Microbiol., 16, 304
Benner, S. A., Devine, K. G., Matveeva, L. N., & Powell, D. H. 2000, PNAS, 97, 2425
Biemann, K., Oro, J., Toulmin, P., III, et al. 1977, JGR, 82, 4641
Briois, C., Thissen, R., Thirkell, L., et al. 2016, P&SS, 131, 33
Bywaters, K., Stoker, C. R., Batista Do Nascimento, N., & Lemke, L. 2020, Life, 10, 12
Cable, M. L., Porco, C., Glein, C. R., et al. 2021, PSJ, 2, 132
Carr, M. H., Belton, M. J. S., Chapman, C. R., et al. 1998, Natur, 391, 363
Carrier, B. l, Beaty, D. w., Meyer, M. a., et al. 2020, AsBio, 20, 785
Cavalazzi, B., & Westall, F. (ed.) 2019, Biosignatures for Astrobiology, Advances in Astrobiology and Biogeophysics (1st ed.; Cham: Springer)
Damer, B., & Deamer, D. 2020, AsBio, 20, 429
de Morais, M., & Teles, A. 2015, in Planetary Exploration and Science: Recent Results and Advances, ed. S. Jin, N. Haghighipour, & W.-H. Ip (Berlin: Springer Geophysics), 147
Deamer, D. 2017, Life, 7, 5
Deamer, D., & Damer, B. 2017, AsBio, 17, 834
European Space Agency 2005, Cosmic Vision: Space Science for Europe 2015–2025 (1st ed.; Amsterdam: ESA)
Fahy, E., Subramaniam, S., Brown, H. A., et al. 2005, J. Lipid Res., 46, 839
Fahy, E., Subramaniam, S., Murphy, R. C., et al. 2009, J. Lipid Res., 50 (Supplement), S9
Georgiou, C. D., & Deamer, D. W. 2014, AsBio, 14, 541
Getty, S. A., Brinckerhoff, W. B., Cornish, T., Ecelberger, S., & Floyd, M. 2012, RCMS, 26, 2786
Goetz, W., Brinckerhoff, W. B., Arevalo, R., et al. 2016, IJAsB, 15, 239
Grasset, O., Dougherty, M. K., Coustenis, A., et al. 2013, P&SS, 78, 1
Grubisic, A., Trainer, M. G., Li, X., et al. 2021, IJMSp, 470, 116707
Hand, K. P., Carlson, R. W., & Chyba, C. F. 2007, AsBio, 7, 1006
Hand, K. P., Murray, A. E., Brinckerhoff, W. B., et al. 2017, The Europa Lander Science Definition Team Report, JPL D-97667, JPL, https://solarsystem.nasa.gov/docs/Europa_Lander_SDT_Report_2016.pdf
Hays, L. E. 2015, NASA Astrobiology Strategy 2015, NASA, https://astrobiology.nasa.gov/uploads/filer_public/01/28/01283266-e401-4dcb-8e05-3918b21edb79/nasa_astrobiology_strategy_2015_151008.pdf
Hoffman, J. H., Griffin, T. P., Limero, T., & Arkin, C. R. 2010, Chapter 31: Space Applications Of Mass Spectrometry, NASA, https://ntrs.nasa.gov/citations/20100039433
Hsu, H.-W., Postberg, F., Sekine, Y., et al. 2015, Natur, 519, 207
Jordan, S. F., Nee, E., & Lane, N. 2019, Interface Focus, 9, 20190067
Kipfer, K. A., Ligterink, N. F. W., Bouwman, J., et al. 2022, PSJ, 3, 43
Kivelson, M. G., Khurana, K. K., Russell, C. T., et al. 2000, Sci, 289, 1340
Klein, H. P. 1979, RvGSP, 17, 1655
Li, X., Danell, R. M., Pinnick, V. T., et al. 2017, IJMSp, 422, 177
Ligterink, N. F. W., Grimaudo, V., Moreno-García, P., et al. 2020a, NatSR, 10, 9641
Ligterink, N. F. W., Kipfer, K. A., Gruchola, S., et al. 2022, Aerospace, 9, 312
Ligterink, N. F. W., Riedo, A., Tulej, M., et al. 2020b, BAAS, 53, 087
Lingam, M., & Loeb, A. 2021, Life in the Cosmos: From Biosignatures to Technosignatures (1st ed.; Cambridge, MA: Harvard Univ. Press)
Lunine, J. I. 2017, AcAau, 131, 123
MacKenzie, S., Neveu, M., Lunine, J. I., et al. 2020, Enceladus Orbilander: A Flagship Mission Concept for the Planetary Decadal Survey, 20205008712, John Hopkins Applied Physics Laboratory, https://ntrs.nasa.gov/citations/20205008712
MacKenzie, S. M., Neveu, M., Davila, A. F., et al. 2021, PSJ, 2, 77
Meyer, S., Riedo, A., Neuland, M. B., Tulej, M., & Wurz, P. 2017, JMSp, 52, 580
Montgomery, W., Jaramillo, E. A., Royle, S. H., et al. 2019, AsBio, 19, 711
Nakatani, Y., Ribeiro, N., Streiff, S., et al. 2014, OLEB, 44, 197
National Academies of Sciences, Engineering, and Medicine 2022, Origins, Worlds, Life: A Decadal Strategy for Planetary Science and Astrobiology 2023-2032 (Washington, DC: The National Academies Press)
National Institute of Standards and Technology 2021a, Phytonadione, NIST Chemistry WebBook, SRD 69, https://webbook.nist.gov/cgi/cbook.cgi?ID=C84800&Mask=200#Mass-Spec

National Institute of Standards and Technology 2021b, Retinol, NIST Chemistry WebBook, SRD 69, https://webbook.nist.gov/cgi/cbook.cgi?ID=C68268&Mask=200#Mass-Spec

National Research Council 2002, A Report Based on the April 2000 Workshop on Life Detection Techniques (Washington, DC: The National Academies Press)

Navarro-González, R., Navarro, K. F., Rosa, J. de la, et al. 2006, PNAS, 103, 16089

Neveu, M., Hays, L. E., Voytek, M. A., New, M. H., & Schulte, M. D. 2018, AsBio, 18, 1375

Onstott, T. C., Ehlmann, B. L., Sapers, H., et al. 2019, AsBio, 19, 1230

Ourisson, G., & Nakatani, Y. 1994, Cell Chem. Biol., 1, 11

Pappalardo, R., Becker, T., Blaney, D., et al. 2021, BAAS, 53, 255

Phillips, C. B., & Pappalardo, R. T. 2014, EOS, 95, 165

Poger, D., & Mark, A. E. 2013, JPCB, 117, 16129

Popa, R. 2004, Between Necessity and Probability: Searching for the Definition and Origin of Life, Advances in Astrobiology and Biogeophysics (1st ed.; Berlin: Springer)

Porco, C. C., Helfenstein, P., Thomas, P. C., et al. 2006, Sci, 311, 1393

Postberg, F., Khawaja, N., Abel, B., et al. 2018, Natur, 558, 564

Postberg, F., Schmidt, J., Hillier, J., Kempf, S., & Srama, R. 2011, Natur, 474, 620

Ray, C., Glein, C. R., Waite, J. H., et al. 2021, Icar, 364, 114248

Riedo, A., Tulej, M., Rohner, U., & Wurz, P. 2017, RScI, 88, 045114

Sáenz, J. P., Sezgin, E., Schwille, P., & Simons, K. 2012, PNAS, 109, 14236

Schulze-Makuch, D., & Irwin, L. N. 2002, AsBio, 2, 105

Schwander, L., Ligterink, N. F. W., Kipfer, K. A., et al. 2022, FrASS, 9, 909193

Sekine, Y., Shibuya, T., Postberg, F., et al. 2015, NatCo, 6, 8604

Selliez, L., Maillard, J., Cherville, B., et al. 2020, RCMS, 34, e8645

Shen, Y., Thiel, V., Suarez-Gonzalez, P., Rampen, S. W., & Reitner, J. 2020, BGeo, 17, 649

Soffen, G. A. 1976, Sci, 194, 1274

Soffen, G. A. 1977, JGR, 82, 3959

Soffen, G. A., & Snyder, C. W. 1976, Sci, 193, 759

Steel, E. L., Davila, A., & McKay, C. P. 2017, AsBio, 17, 862

Vago, J. L., Westall, F., Pasteur Instrument Teams, et al. 2017, AsBio, 17, 471

Voyage 2050 Senior Committee 2021, Voyage 2050 Final Recommendations (Paris: ESA), https://www.cosmos.esa.int/documents/1866264/1866292/Voyage2050-Senior-Committee-report-public.pdf/e2b2631e-5348-5d2d-60c1-437225981b6b?t=1623427287109

Waite, J. H., Glein, C. R., Perryman, R. S., et al. 2017, Sci, 356, 155

Waite, J. H., Jr., Combi, M. R., Ip, W.-H., et al. 2006, Sci, 311, 1419

Waite, J. H., Jr., Lewis, W. S., Magee, B. A., et al. 2009, Natur, 460, 487

Waldbauer, J. R., Newman, D. K., & Summons, R. E. 2011, PNAS, 108, 13409

Wilhelm, M. B., Ricco, A. J., Chin, M., et al. 2020, LPI Contribution, 2241, 5116

Willhite, L., Ni, Z., Arevalo, R., et al. 2021, in 2021 IEEE Aerospace Conf. (Piscataway, NJ: IEEE), 1